# Compact steep spectrum 3CR radio sources. VLBI observations at 18 cm

C. Fanti<sup>1,2</sup>, R. Fanti<sup>1,2</sup>, P. Parma<sup>1</sup>, R. T. Schilizzi<sup>3</sup>, and W. J. M. van Breugel<sup>4</sup>

- <sup>1</sup> Istituto di Radioastronomia del CNR, Via Irnerio 46, I-40126 Bologna, Italy
- <sup>2</sup> Dipartimento di Astronomia, Università di Bologna, Italy
- <sup>3</sup> Netherlands Foundation for Radioastronomy, Dwingeloo, The Netherlands
- <sup>4</sup> Radio Astronomy Laboratory, University of California Berkeley, USA

Received July 9, accepted September 21, 1984

Summary. We present the first results of a program to investigate the kiloparsec sized radio structure of a representative sample of Compact Steep Spectrum (CSS) sources from the 3CR catalogue. Ten objects (3C 49, 67, 119, 237, 241, 268.3, 287, 303.1, 343, 343.1) have been mapped at 18 cm with a resolution of ~30 milli-arc s (mas) using the European VLBI Network (EVN). In some cases the VLBI data have been supplemented by MERLIN observations at the same wavelength to enhance sensitivity to large scale structure.

The overall sizes of CSS sources we observed range from about 100 mas to 1 or 2", corresponding to linear sizes of the order of 1 to 10 kpc. The morphological classification ranges from double, to "core-jet", to complex; CSS quasars are generally "core-jets" or complex, while CSS radio galaxies are doubles, although not necessarily simple doubles.

**Key words:** compact steep spectrum radio sources – quasars – radio galaxies – VLBI

### 1. Introduction

In recent years, compact steep spectrum (CSS) sources have come to be recognized as a third class of radio source in addition to the classical steep spectrum double and the compact flat spectrum sources (Bridle and Fomalont, 1978; Miley, 1980; Peacock and Wall, 1982). Their chief characteristics are: (i) physical sizes of the order of a few kpc, and (ii) the absence of a dominant flat spectrum radio core.

Systematic radio studies of this class of object have been carried out by Kapahi (1981), Peacock and Wall (1982) and van Breugel, Miley and Heckman (1984c; hereafter vBMH). The latter study, using the VLA at 2 and 6 cm with resolutions of 150 and 400 mas, discerned that CSS sources in general have complex morphology on the kpc scale, high surface brightness and low percentage polarization. Information at even higher resolution is available only for a few of the strongest members of this class: 3C 48, 3C 138, 3C 147, 3C 286, 3C 309.1, and 3C 380 (see references in Table 1). All display an elongated "core-jet like" structure on angular scales of ten to a few hundred mas, a morphology reminiscent of the compact flat spectrum sources, but with the difference that here the core is not dominant at high frequencies.

Send offprint requests to: C. Fanti

In a number of steep spectrum sources of small linear size, close enough to allow a very detailed structural analysis, morphological relations have been found between the radio total intensity and polarization distribution, and the distribution of optical line emission in the narrow (forbidden) line region (NLR) (e.g. Miley, 1981; Heckman et al., 1982; vBMH). In addition there are correlations linking the radio luminosity of the steep spectrum cores in Seyfert galaxies with the NLR [O III]  $\lambda$  5007 luminosity (de Bruyn and Wilson, 1978) and line-width (Wilson and Willis, 1980; Heckman et al., 1981).

Heckman et al. (1982), van Breugel et al. (1984a, b) and vBMH have suggested that also for the CSS sources, even in the most powerful quasars, many of the radio and optical properties may be understood as being due to jets propagating through dense and inhomogeneous interstellar media. It is therefore of considerable interest for our understanding of the evolution of radio sources in the nuclear environment of the underlying optical object, to continue the systematic study of these sources at higher resolution and particularly at a resolution matching that of the future Hubble Space Telescope.

For some years now we have been carrying out such a study for a sample of CSS sources in the 3CR catalogue utilising both VLBI and MERLIN observations at 18 cm. Complementary VLA observations at higher frequencies ( $\lambda \lesssim 6$  cm) have already been published (vBMH) or have been carried out recently (van Breugel et al., in preparation). In this paper we present VLBI observations of 10 of such sources.

## 2. Definition of a CSS source and of the sample

The fact that the angular resolution of a radiotelescope is often inadequate with respect to the physical size of radio sources has led to the loose definition that CSS sources are bright objects of relatively small angular size (less than a few arcseconds) having normal power-law spectra [typically  $\alpha \sim 0.7 \pm 0.2$ ,  $S(\nu) \propto \nu^{-\alpha}$ ] over the entire observed radio frequency range, except for possibly a low frequency turn-over around or below 1 GHz.

Because of the above mentioned relationships between radio and optical properties found in several nearby CSS radio sources, we think it is more appropriate to use a physically more meaningful selection criterion, which emphasizes small *linear* (i.e. much less than a typical galactic diameter) rather than *angular* size (van Breugel, 1984). With such a choice, some weak, low surface brightness *nearby* objects, such as, for instance, M84 and M87

Table 1. The 3CR sample of CSS sources

3C	$S_{178}$	Z	Radio spectrum	${\rm Log}_{P_{178}}$	Id. (m <sub>v</sub> )	Overall size		Map references	
						(arcs)	(kpc)	(arc s)	(subarcs)
43	11.6	1.457	0.71 S	28.4	Q(20.0)	< 1.5	< 6.0		
48	55.0	0.367	0.80C-	27.9	Q(16.2)	0.33	1.0		1, 19
49	10.3	0.621	0.81 <i>C</i> —	27.6	G(22.0)	1.0	3.5	C	6
67	10.0	0.310	0.83C-	27.0	G(18.0)	2.3	6.2	C, vB	6, 19
138	22.2	0.759	0.56C-	28.1	Q(17.9)	0.42	1.5		10a, 19
147	60.5	0.545	0.74C-	28.3	Q(16.9)	0.7	2.4		2, 3, 4, 8, 11
									15, 17, 18, 19
190	15.0	1.197	0.86  S	28.3	Q(20.0)	2.4	9.0	L	
216	20.2	0.668	0.65 S	28.0	$\widetilde{Q}(18.5)$	0.8	3.0	PR	16b
241	11.6	1.617	1.14C-	28.5	$\widetilde{G}(>22)$	0.9	3.2	C	6
268.3	10.7	0.371	0.85C-	27.2	G(19.0)	1.56	4.4	C, vB	6, 19
286	25.0	0.849	0.47 <i>C</i> —	28.3	Q(17.3)	2.6	9.7	C, vB	2, 5, 7, 10b 15
287	16.3	1.055	0.58C-	28.3	Q(17.7)	0.1	0.4		6
299 .	11.8	0.367	0.88 <i>C</i> —	27.2	G(19.5)	11.5	34.0	JPR, L, C, vB	
303.1	8.1	0.267	1.07 C -	26.8	G(19.0)	1.8	4.5	Ć	6
305.1	4.6	1.4	0.92C-	28.0	G(21.0)	2.3	8.4	C	
309.1	22.7	0.904	0.57 S	28.3	Q(16.8)	2.1	7.8	L, vB, W PR	9, 14, 16b, 19
318	12.3	0.752	0.92 <i>C</i> –	27.8	G(20.3)	< 0.2	< 0.7		
343	12.4	0.988	0.84C-	28.1	Q(20.6)	0.25	0.7		6
343.1	11.5	0.750	0.99 C	27.8	G(20.8)	0.38	1.3		6, 19
346	10.9	0.161	0.65S	26.5	G(17.2)	8.0	14.0	JPR	• • • • • • • • • • • • • • • • • • • •
380	59.7	0.691	0.71 S	28.5	Q(16.8)	3.8	13.8	L, W, PR	8, 9, 13a, 15, 16a, b
454	11.6	1.757	0.76  S	28.6	Q(18.5)	< 1.3	< 4.5	L	,
119	15.7	0.408	0.66C-	27.4	$\widetilde{Q}(20.0)$	0.23	0.9		6, 7
237	20.9	(0.5?)	0.74C-	(27.7)	$\widetilde{EF}(>20)$	1.4	(4.7)	C	6
298	47.5	1.439	1.05 <i>C</i> –	29.0	Q(16.8)	2.0	7.3	C	12

# References for Table 1

Fluxes at 178 MHz and optical data are mostly from Laing et al. (1983); redshift for 3C 241 and 3C 305.1 from Spinrad (private communication)

Ref. for radio structure  Arcsec structure  JPR: Jenkins et al. (1977)  PR: Pearson and Readhead (1984)  C: Charlsworth et al. (in preparation)  W: Wilkinson et al. (1984a, b)  L: Laing (1981)  vB: van Breugel et al. (1984c)	5 GHz 5 GHz 1.6 GHz 1.6/5 GHz 5/15 GHz 5/15 GHz	6) Present paper 7) Pearson et al. (1980) 8) Readhead and Wilkinson (1980) 9) Wilkinson (1982) 10a) Geldzahler et al. (1984a) 10b) Geldzahler et al. (1984b, in preparation) 11) Simon et al. (1984) 12) Graham and Matveienko (1984) 13) Wilkinson et al. (1984a) 14) Kus et al. (1981) 15) Phillips and Shaffer (1983)	1.6 GHz 1.6 GHz 1.6 GHz 1.6 GHz 1.6 GHz 1.6 GHz 1.6 GHz 1.6 GHz 1.6 GHz 2.3 GHz
<ol> <li>Wilkinson et al. (1984b)</li> <li>Simon et al. (1980)</li> <li>Simon et al. (1983)</li> <li>Wilkinson et al. (1977)</li> <li>Wilkinson and Readhead (1979)</li> </ol>	0.3 GHz 0.3 GHz 0.3 GHz 0.6 GHz 0.6 GHz	16a) Pearson and Readhead (1981) 16b) Pearson and Readhead (1984) 17) Preuss et al. (1982) 18) Preuss et al. (1984) 19) van Breugel et al. (1984c)	5.0 GHz 5.0 GHz 5.0 GHz 5.0 GHz 15.0 GHz

(giant ellipticals of the Virgo cluster), M 82 (a starburst galaxy) or NGC 1068 (spiral-Seyfert galaxy) may also be classified as Compact Steep Spectrum radio sources in spite of their large angular extent. These closer objects can be studied in great detail at all wavelengths and are favoured candidates for comparative optical and radio studies.

In this paper we define as CSS those radio sources which have most (i.e. at least 80%) of their flux density at 5 GHz in a steep (i.e.  $\alpha$ >0.5 above  $\sim$ 0.4 GHz) straight spectrum component of subgalactic dimension, i.e. with projected linear size less than 10 kpc ( $H_0$ =100 km s<sup>-1</sup>/Mpc,  $q_0$ =1).

The actual limits here are slightly arbitrary, and are chosen to obtain a complete sample which emphasizes the most important characteristics of these objects. In particular, the limiting value adopted for the linear size is aimed at preventing too heavy a contamination of the sample due to intrinsically large radio sources which appear small only because of projection effects.

To rigorously select such a sample from existing radio source catalogues, relatively high resolution (a few arcseconds) radio maps are required. Such data are avaiable for the "complete" 3CR sub-sample (referred to as 166-3CR) which consists of 166 members all mapped with the Cambridge 5 km telescope (Jenkins et al., 1977). Because selection of sources from the 166-3CR sample is based on maps of only moderate dynamic range and sensitivity, it is possibly not as sharp as desired. We cannot exclude the possibility that, in some cases, extended low brightness emission has been missed. Good examples in this respect are 3C 293, where extensive low surface brightness lobes are visible, in more recent maps, in addition to the CSS component (Bridle et al., 1981) or 3C 236, the largest galaxy known (Barthel et al., 1984). Note however, that 3C 236 does not belong to our sample because it has less than 80% of its total flux density in a compact feature.

Finally our selection could also be biased by spectral variations. However, since all objects in our sample have a steep spectrum over a fairly large frequency range from  $\sim 0.4$  GHz to 5 GHz (Kellermann et al., 1969; Kuhr et al., 1979), we believe this effect to be unimportant.

In this paper, we limit our analysis to the most powerful radio sources  $(P(178) \ge 10^{26} \text{ W/Hz})$  in the 166-3CR sample which meet the above constraints. This results in the exclusion of a few objects: 3C 231 (M 82), 3C 272.1 (M 84), 3C 274 (M 87), 3C 293, and 3C 305. Some of these weaker sources might be governed by processes different from those acting in the more powerful CSS radio sources, although a physical link between them has been suggested by vBMH. Furthermore we added 3C 119, 3C 237, 3C 298, which are not members of the 166-3CR sample but are known to be CSS.

The 25 objects in such a list are given in Table 1 together with some general information. We note that only a few objects (3C 147, 3C 216, 3C 309.1, 3C 343, and 3C 380) are common to the survey list of Pearson and Readhead (1984). This is not surprising since these authors selected the sources at 5 GHz, so that strong flat-spectrum objects are favoured.

The limiting linear size chosen coupled with the cut-off in radio power results in an overall angular extent for the compact features in the sample of less than 2–3". Sources up to this angular size can be mapped with the EVN, provided they have sub-structures smaller than 100 mas. We began by observing those sources of Table 1 which show a well defined low frequency turnover, or at least a clear flattening in their spectrum. If this bending in the spectrum is due to synchrotron self-absorption, this provides, in fact, a good indication of the presence of substructure of the proper size to be mapped with the EVN. These sources (18) are indicated

by C- in Table 1. The present status of the VLBI observations for the whole sample can be ascertained from the references in the last column of Table 1.

#### 3. Observations and data reduction

The observations were made with telescopes at Onsala (ON), Effelsberg (EF), Dwingeloo (DW), and Jodrell Bank MK-IA (JO) at 1660 MHz, in left circular polarization. Two antennas of the Westerbork telescope (WS) were used in tied-array mode instead of Dwingeloo for the observations of 3C 67, 3C 119 and three for 3C 268.3. The synthesized beam size depends on the source declination, and ranges from  $\sim\!25\times25\,\mathrm{mas}$  to  $\sim\!40\times30\,\mathrm{mas}$ . The observations cover the period October 1981–October 1983 and the date at which each source was observed is given in Table 2. Each source was tracked for 10–12 h, and observations interleaved with short scans on calibration sources.

The signals were recorded with the standard Mk-II VLBI system with a 1.8 MHz bandwidth; correlation was carried out at the Max-Planck-Institut für Radioastronomie in Bonn.

Many of the sources have complex morphology causing rapid changes in the visibility function even on the shortest baseline. In order not to lose structural information, the data were therefore coherently averaged for two minutes only. This implied that in some cases the signal-to-noise ratio was poor for short intervals of time on some of the longest baselines. Only 3C 303.1 was so weak on all baselines that it was necessary to integrate for 8 min in order to have a sufficiently high signal-to-noise ratio.

For a 2-min integration the signal attenuation due to coherence losses was negligible, whilst for the 8-min integration a correction had to be applied to the data. Typical noise values (1 r.m.s.) for a 2-min integration are 15, 40, 20, 20, 10, 25 mJy for the baselines ON-EF, ON-DW, ON-JO, EF-DW, EF-JO, DW-JO respectively. When Westerbork was used instead of Dwingeloo, the noise for the corresponding baselines decreased by ~10%.

The correlated flux scale was calibrated following Cohen et al. (1975) using OQ 208, 0235+164 and DA 193, which are believed to be essentially unresolved at these spacings and whose flux densities were measured at Effelsberg during the observations. The internal consistency of the calibration factors for each baseline is generally better than 3% (1 r.m.s.).

After preliminary model fitting of the visibility amplitudes to provide a reliable starting model, we produced hybrid maps using the CORTEL program (Cornwell and Wilkinson, 1981) as the first step of the procedure. Iterations halted when the visibility amplitudes and closure phases of the model showed good agreement with the data. A redundant but useful check was to also compare the model phases with the "corrected" ones for each baseline, which allowed removal of isolated bad points which are easily recognizable in this way. The dynamic range achieved ranged from better than 100 to 1 in the best cases (e.g. 3C 49 and 3C 119) to about 30 to 1 in the worst cases (e.g. 3C 343). These figures are always worse than expected from the theoretical noise on the map. The final hybrid maps were further analyzed to obtain the component parameters and the overall noise in the map (Table 2).

For all the sources for which we had access to MERLIN data, we produced new hybrid maps combining the EVN data with those of four MERLIN telescopes, Mk II, Wardle, Knockin, and Defford (Davies et al., 1980). This required careful matching of the flux scales before combination. In no case did the flux vary between the two epochs of measurement with MERLIN and EVN,

Table 2. VLBI data from the present paper

3C name	Total flux mJy	Component	VLBI flux mJy	Size	Total size	Overall map noise	Obs. date	
				mas	p.a.	arc s	mJy/beam	uaic
3C 49	2310	E W compact W diffuse	1550 130 620*	22 × 12! 45 × 25! 220 × 110*	(94) (60) (80)	1.01	1.7	Oct. 82
3C 67	2650	N S compact S halo	~ 900* 280 ~1200*	$\sim 500 \times 150*$ $60 \times 25!$ $330 \times 200*$	(24)	2.3	0.8	Oct. 83
3C 119	8060	N S "halo"	4200 1300 ∼2400*	$15 \times 6!$ $28 \times 11!$ $> 230 \times 150*$	(55) (105) (90)	0.23	3.0	Oct. 83
3C 237	5580	W E	3310* 2250*	$360 \times 170*$ $350 \times 210*$	(80) (80)	1.40	2.5	Apr. 82
3C 241	1400	W-west bridge east E	480 80 110 570	$60 \times 35!$ 50 $35 \times 15!$ $60 \times 30!$	(135) (67) (116)	0.91	0.8	Oct. 82
3C 268.3	3250	N compact n-jet s-jet halo S	140 410 80 ~1550* ~1100*	$30 \times 14!$ $95 \times 40!$ 70! $220 \times 160*$ $400 \times 140*$	(64) (160) (150) (150)	1.56	0.7	Apr. 83
3C 287	6240		6180	> 80 × 70	` ,	0.09	4.5	Oct. 81
3C 303.1	1480	Elliptical Knot 1 Knot 2 Knot 3 Diff. em.	580 82 54 45 600*	$100 \times 40!$ $40 \times 24!$ $32 \times < 6!$ $14 \times < 6!$ $500 \times 150*$	(126) (48) (35) (148)	1.8	0.5	Oct. 82
3C 343	4310	Main comp. N	4200 110	$170\times140$		0.25	5.0	Apr. 82
3C 343.1	3890	W E	2460 1060	$170 \times 110$ $130 \times 70$	(90) (120)	0.38	2.0	Apr. 82

Notes:

Total flux density, measured at Effelsberg simultaneously with the EVN observations.

a fact which allowed us to assume that the structure itself did not vary. The combined data provide a much better u-v coverage since they fill the gap at short baselines (from  $\sim 0.16$  to  $\sim 0.7$  M-lambda; see Sect. 4) thereby allowing us to map low brightness extended features which are not well reproduced with the EVN data alone.

In most cases this procedure did not change the general description of structure, but for a few objects the improvement in map quality is remarkable. In these cases also the combined map is shown together with the one obtained with only the EVN data.

## 4. Map reliability

Because the large extent of some radio sources in the sample appears to exceed the field of view derived from the available u-v coverage, a few comments on structure reliability are needed.

The classical sampling theorem (Bracewell, 1954) states that if the u-v plane is regularly sampled at intervals  $\Delta uv$ , then the mappable field of view is  $1/\Delta uv$ . This theorem however does not consider image reconstruction algorithms, like CLEAN, which perform an interpolation in the u-v plane, allowing satisfactory image reconstruction from largely undersampled u-v data. WSRT and VLA maps are good examples of this.

VLBI observations are not as well off, in view of the large and irregular gaps in the u-v coverage. In our observations we have substantial holes around the origin of the u-v plane (baselines up to  $\sim 1$  M-lambda) and between the baselines EF-DW and DW-ON or DW-JO (or the equivalent with WS), from  $\sim 1$  to  $\sim 3$  M-lambda. These gaps imply that any round gaussian source with HPW greater than  $\sim 50$  mas is difficult to reconstruct, since it is sampled properly only by the innermost baseline, while gaussian sources larger than 100 mas (HPW) are irretrievably lost.

<sup>!:</sup> FWHM (deconvolved for the restoring beam) of the gaussian component best-fitting the map data; otherwise the diameter is estimated from the lowest reliable contour;

<sup>\*:</sup> Data are from the combined EVN+MERLIN map

Well separated double sources, with individual components  $<50-100\,\mathrm{mas}$  do not give serious problems, since the double structure may be well sampled along each u-v track. The limitation, in this case, is set by the component intensities: widely separated components may produce modulations in the visibility amplitude with "periods" comparable to, or faster than, the integration time required to detect the signal. In this case the structural information is lost or degraded. With the telescope configuration at our disposal, double sources with separation larger than 2" gave problems unless they had a high flux density.

These limitations coincide more or less with the practical rules enunciated by Wilkinson (1983), provided one applies them to the size of the individual sub-components mapped and allow the total field of view to be much larger. Fortunately no source is just a smooth round gaussian, so that the above considerations are somewhat pessimistic and should be considered mainly as a warning.

In order to evaluate the reliability of the structures, we have analyzed the visibility amplitudes as a function of the sampled baseline in order to decide if, in some cases, any information has been lost. For example, in sources like 3C 67 or 3C 268.3 (see next section) the reconstruction methods are unable to extrapolate properly to zero baseline from the information present in the VLBI observations alone. In order to obtain an acceptable map it was necessary to add a few shorter baselines to sample the central u-v gap. We did so using MERLIN observations, kindly made available to us by Drs. R. E. Spencer and M. Charlsworth.

Another difficult source to map with the VLBI data alone is 3C 343. In this case, the shortest baseline (EF-DW) is sensitive to a large fraction of the total flux density ( $\sim$ 2-4 Jy), whilst the remaining ones "see" at most 1 Jy. In such a case, there is no great need for adding shorter baselines, while baselines ranging from 1 to 3 M-lambda would be valuable in order to improve the u-v coverage and allow mapping of the source. Unfortunately the required baselines are not available.

Some further remarks have to do with the adopted reconstruction algorithms. For very complex sources, map production is by no means automatic with 6 baselines only, and one has to interact with the procedure while it converges, checking the "model" against the observed complex visibilities. The choice of the CLEAN window, as well as the selection of the CLEAN components to be entered in CORTEL, has to be done with care. Sometimes it is necessary to exclude from the search area regions occupied by particularly strong sidelobes. This of course prevents the detection of any true emission originating in those areas.

The final remark concerns the amplitude corrections at the telescopes, allowed for by the CORTEL procedure. We realized, "a posteriori", that with only four telescopes observing complex sources there are not enough constraints to solve unambiguously for both telescope gain corrections and source structure. It is possible to get convergence of the iterative procedure and a good fit to the data with large gain corrections (up to 10-20%) and suppression (or invention) of weak, poorly sampled radio components, which would easily show up in maps with better u-v data. The best example of this is 3C 237. Here the EVN data alone allowed us to obtain a map which could fit the data well, at the expense of gain corrections of sometimes up to 20% which depress visibility amplitudes marginally sensitive to very poorly sampled broad components. After adding shorter baselines from MERLIN to the EVN data we could produce a map whose components fit the EVN data with negligible (<5%) gain correction. For these reasons we adopted the conservative approach of trusting the

amplitude calibration and applying no telescope gain corrections at all.

For the sources which proved most difficult to map we display plots of the visibility amplitudes and closure phases, in order to show how the final solution fits the original data and to enable the reader to evaluate the reliability of the maps.

#### 5. Comments on individual sources

Measured parameters of the observed sources are given in Table 2. Total radio spectra are shown in Fig. 1, hybrid maps in Figs. 2–11, and some of the visibility plots in Fig. 12. In all maps except 3C 303.1 north is up and East to left. The restoring beam (FWHP) is represented by the shaded ellipse in the lower left hand corner. Contours (mJy/beam) are given in the figure captions. Only for the weakest sources does the noise level (Table 2) become relatively important and influences the reliability of structural details.

3C 49: The EVN map shows a very simple structure (Fig. 2a), consisting of two well separated components of very different surface brightness. The brighter component in the west is barely resolved at the present EVN resolution. A combination of EVN and MERLIN data demonstrates that the eastern component is a knot (maybe a hot spot) of an extended, bent, low brightness feature (Fig. 2b). The flux density in the combined map is within a few percent of the single dish flux density measured at Effelsberg during the observations.

Lower resolution lunar occultation measurements at 327 MHz by Joshi and Gopal-Krishna (1977) are consistent with the VLBI structure, as are VLBI measurements by Broderick and Condon (1975) at 430 MHz and Clark et al. (1975) at 111 and 197 MHz. Combining our data with that of Broderick and Condon (1975) and Clark et al. (1975), it is possible to derive the rough behaviour of the spectra for the "compact" western component and for the extended eastern one. The eastern component has a straight spectrum with slope ~1.1 while the spectrum of the western component appears to peak around 1 GHz. This is confirmed by snap-shot EVN observations made by us at 5 GHz. The asymmetry between the two components suggests that we are not dealing with a classical double source of small dimensions, but rather with a D2 type double (McDonald and Miley, 1971) or a "core-jet" with the "core" located in the western component.

3C67: In the VLA maps by vBMH the source displays a double structure with separation of 2"3.

The EVN observations largely resolve the structure and account for only a small fraction of the total flux:  $\sim\!20\%$  in E-W, and  $<\!10\%$  in the remaining baselines. Rapid beating in the three baselines E-W, E-J, and W-J (Fig. 12a), however, indicates that compact features are present in both components.

A good EVN map of the whole source cannot be produced owing to insufficient u, v coverage. A poor quality map of the southern component is shown in Fig. 3a). It consists of an elliptical component of  $60 \times 25$  mas in p.a. 24 deg, with S type shape, and three other lower brightness features, which form a sort of ring. Figure 3b shows the map obtained by combining the EVN and MERLIN data. The two main components are now both visible and account for about 90% of the source total flux density. The northern component is of quite low surface brightness with several smooth sub-condensations. In the southern component (Fig. 3c) the bright features seen in the EVN map are well recognizable embedded in a broader low surface brightness structure ("halo"). The two major components have different degrees of polarization (vBMH) the northern one being definitely polarized. Both have a

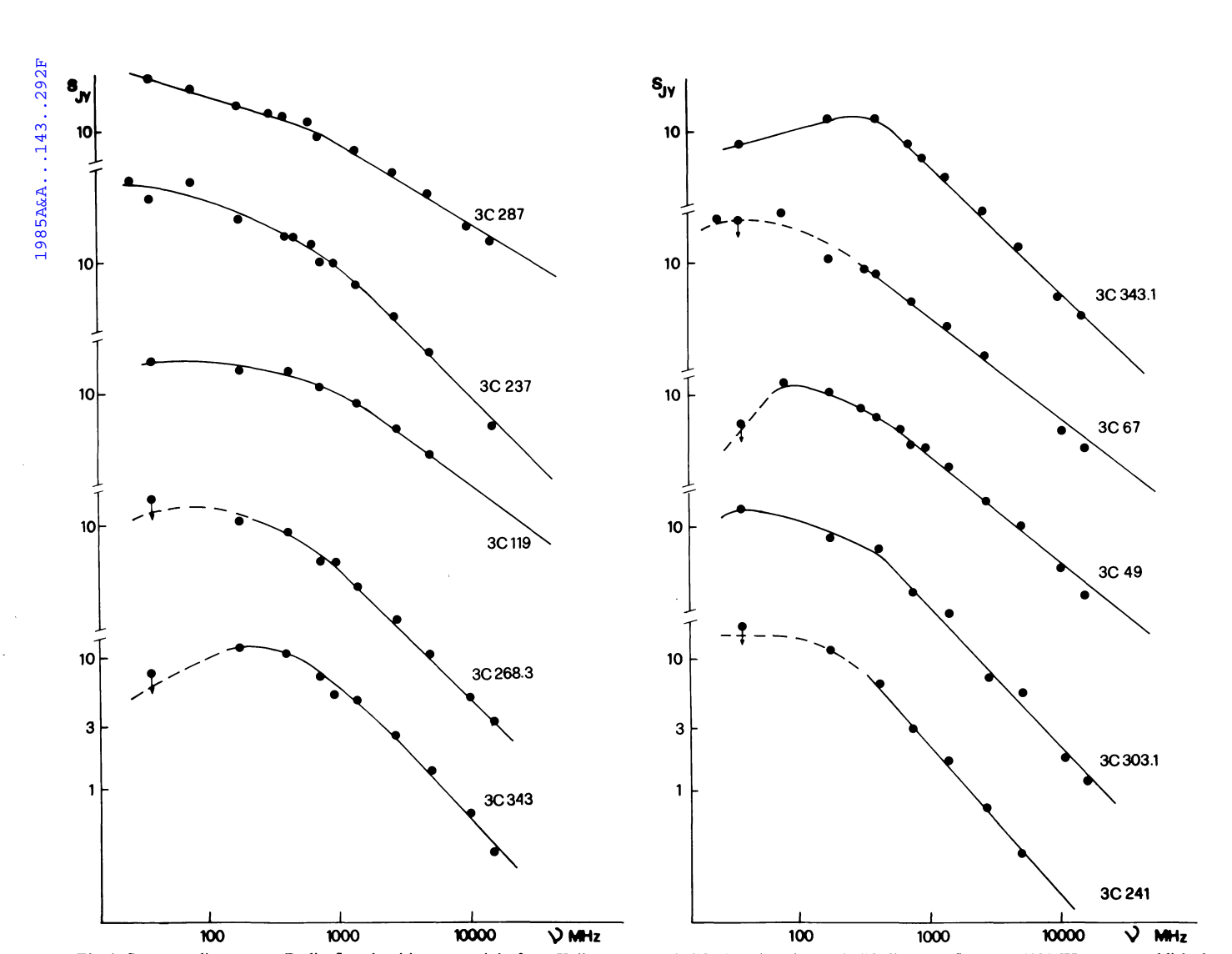


Fig. 1. Source radio spectra. Radio flux densities are mainly from Kellermann et al. (1969) and Kuhr et al. (1979). Most fluxes at 408 MHz are unpublished measurements from the East-West arm of the Bologna Cross

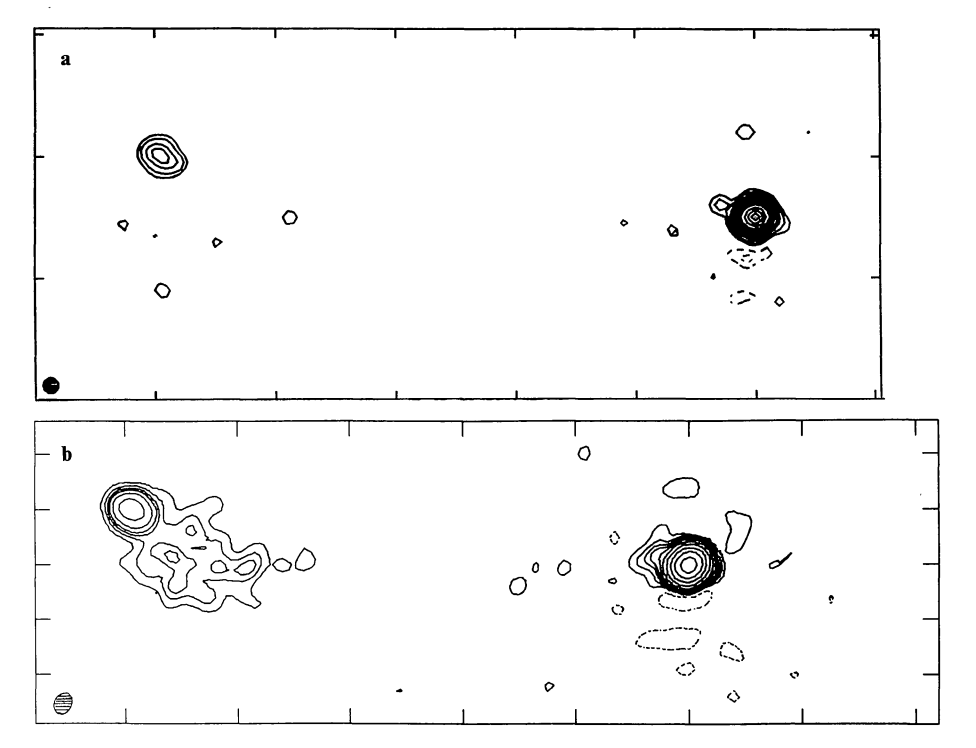


Fig. 2a and b. Brightness distribution at 1.6 GHz of 3C 49. a EVN data; beam:  $25 \times 25$  mas; tick separation: 200 mas; contours:  $11 \times (-1, -0.5, 0.5, 1, 2, 3, 4, 6, 8, 10, 15, 20, 40, 60, 80, 100)$  mJy/beam; peak flux: 1110 mJy/beam. b EVN+MERLIN data; beam:  $37 \times 31$  (p.a. = -22) mas; tick separation: 200 mas in R.A., 100 mas in dec.; contours:  $5 \times (-1, 1, 2, 3, 4, 6, 10, 20, 40, 80, 160, 240)$  mJy/beam; peak flux: 1200 mJy/beam

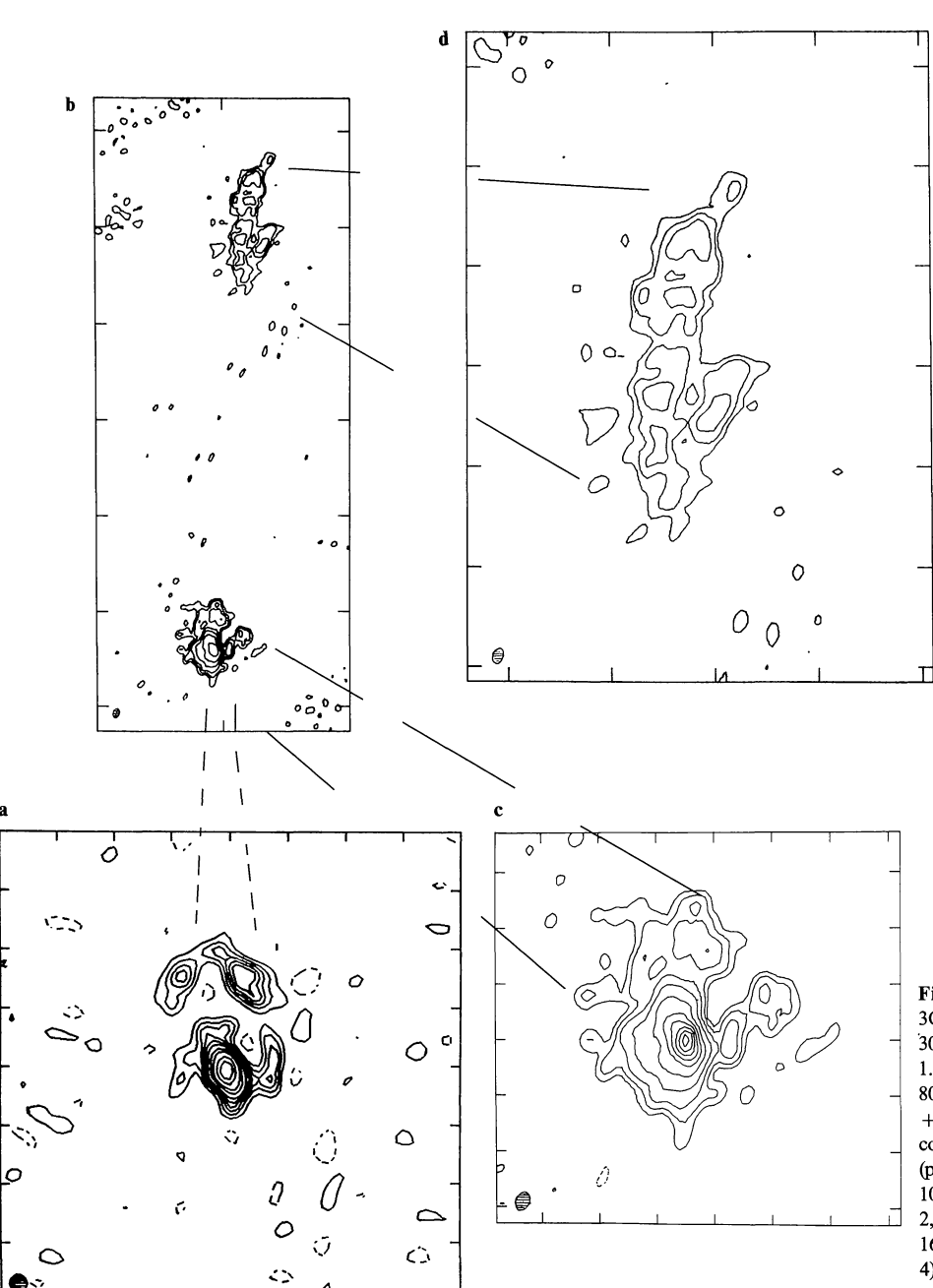


Fig. 3a-d. Brightness distribution at 1.6 GHz of  $3C\,67$ . a EVN data (southern component); beam:  $30\times30$  mas; tick separation: 100 mas; contours:  $1.1\times(-3,3,6,9,12,15,20,30,40,60,80)$  mJy/beam; peak flux: 108 mJy/beam. b-d EVN + MERLIN data: b whole source, c southern component, d northern component; beam  $34\times26$  (p.a. = -19) mas; tick separation: 500 mas in b, 100 mas in c, 200 mas in d; contours:  $2.5\times(-1,1,2,4,8,16,32)$  mJy/beam in b;  $2.5\times(-1,1,2,4,8,16,32,40,48,56)$  mJy/beam in c;  $2.5\times(1,2,4,8,16,32,40,48,56)$  mJy/beam in d; peak flux: 155 mJy/beam in b and c; 15 mJy/beam in d

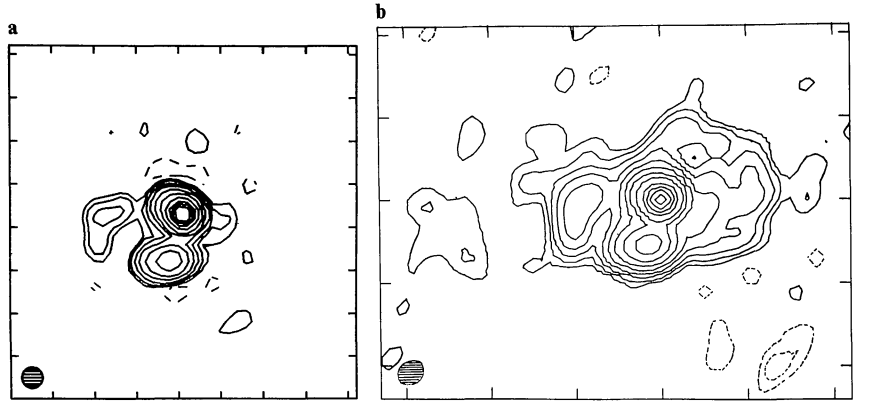


Fig. 4a and b. Brightness distribution at 1.6 GHz of 3C 119. a EVN data; beam:  $25 \times 25$  mas; tick separation: 50 mas; contours:  $30 \times (-0.5, 0.5, 1, 2, 4, 8, 16, 32, 48, 64, 80)$  mJy/beam; peak flux: 3050 mJy/beam. b EVN + MERLIN data: beam  $30 \times 28$  (p.a. = -55) mas; tick separation: 100 mas; contours:  $5 \times (-2, -1, 1, 2, 4, 8, 16, 32, 64, 128, 256, 384, 512, 640)$  mJy/beam; peak flux: 3840 mJy/beam

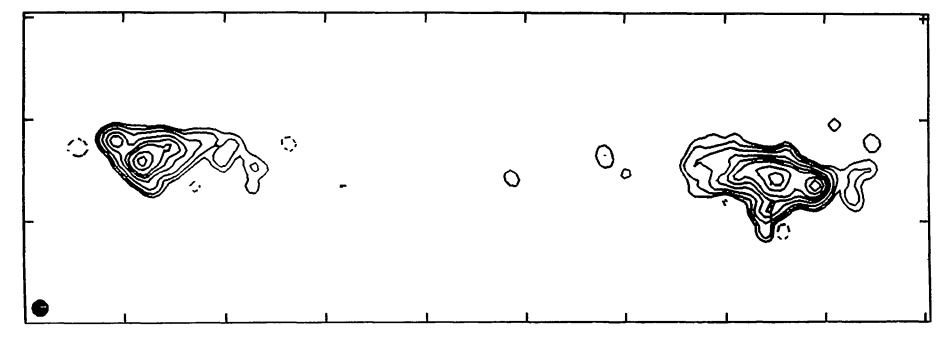


Fig. 5. Brightness distribution at 1.6 GHz of 3C 237. Beam:  $30 \times 30$  mas; tick separation: 200 mas; contours:  $2.7 \times (-2.5, 2.5, 5, 7.5, 10, 15, 20, 30, 40, 60, 80)$  mJy/beam; peak flux: 270 mJy/beam

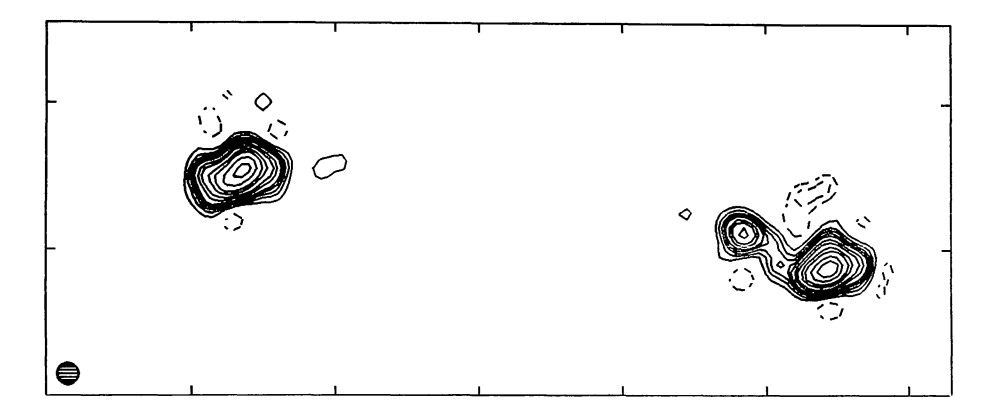


Fig. 6. Brightness distribution at 1.6 GHz of 3C 241. Beam:  $30 \times 30$  mas; tick separation: 200 mas; contours:  $2 \times (-4, -2, 2, 4, 6, 8, 10, 15, 20, 30, 40, 60, 80)$  mJy/beam; peak flux: 200 mJy/beam

straight steep spectrum from 18 to 2 cm. ( $\alpha \sim 0.95$  in the northern, 0.78 in the southern.)

The optical position of the suggested identification (Laing et al., 1983) coincides, within the errors, with that of the southern component. Therefore the source is a D2 type double and we are led to identify the bright feature of the southern component with the radio "core".

 $3C\,119$ : The main structure seen from our observations (Fig. 4a) is a double separated by  $\sim 56\,\mathrm{mas}$  along p.a. 164 deg, which accounts for  $\sim 70\,\%$  of the total flux density. Both components appear resolved at our resolution. The brighter northern component is extended by  $\sim 15\,\mathrm{mas}$  along p.a. 55 deg. Earlier VLBI observations (Pearson et al., 1980) at the same frequency, but with higher resolution ( $5\times 10\,\mathrm{mas}$ ), failed to detect the southern component, but resolved the northern one into a double with a bright component of  $\sim 2.5\,\mathrm{Jy}$  separated by 20 mas in p.a.  $\sim 50^\circ$  from a component of  $\sim 0.5\,\mathrm{Jy}$ , in agreement with the extension we find.

A MERLIN map with about 200 mas resolution, accounts for the total flux density (Charlsworth et al., in preparation) but is elongated in a totally different direction (p.a.  $\sim 100 \, \mathrm{deg}$ ), in agreement with the VLA observations of vBMH. A combined EVN+MERLIN map is shown in Fig. 4b where the larger scale emission at p.a.  $\sim 100 \, \mathrm{deg}$ , referred to as "halo", is clearly visible. Hints of this broad feature are also seen (at 1% level) on the EVN map by itself. It seems difficult to reconcile our results with those at 408 MHz of Clark et al. (1969), where separations of 290 mas in p.a.  $\sim 10 \, \mathrm{deg}$ , or 140 mas in p.a. 30 deg or 140 deg were found.

 $3C\,237$ : The source consists of two well spaced radio components of similar flux and size (Fig. 5). Both contain high brightness sub-components. In the EVN map  $\sim 40\%$  of the total flux density is missing. When combining EVN and MERLIN data, low brightness envelopes show up, in both components, but mainly in the eastern one, although the general structure does not change.

In this combined map (not shown) the integrated flux density fully accounts for that measured with single dish. The ratio (separation)/(component transverse size) is large (>20). If this source were a several kpc double, aligned close to the line of sight so as to show a small angular size because of projection effects, the deprojected ratio would be extremely large. Therefore we prefer to consider 3C 237 a scaled down version (by more than a factor 100 in linear size), but of similar radio power, of a classical strong double source (e.g. Cygnus A). A curious radio feature, transverse to the main overall radio axis, is visible close to the mid point of the western component, where also a bright knot is visible. Finally we do not detect any compact nuclear component between the radio lobes, at a level 5% of the peak (<14 mJy). In the relativistic beaming model (Scheuer and Readhead, 1979) the absence of any core could be further argument for a large angle to the line of sight.

3C 241: "Double" source (Fig. 6). The western component is itself split into two parts connected by a bridge of emission; the eastern component is somewhat extended. The two outermost components are very similar in flux density, size, and orientation. The integrated flux density is  $\sim 90\%$  of the single dish measure. The appearance of the combined EVN+MERLIN map (not shown) is very similar to this one and the total flux density is accounted for.

3C 268.3: In lower resolution observations (e.g. vBHM) the source appears as a double with a separation of 1".5, the northern component being the stronger one. At the EVN resolution the southern component is of such a low and uniform surface brightness that it cannot be mapped, although its presence is revealed by modulations in the visibility amplitudes of E-W, E-J, and W-J (Fig. 12b). The northern component, on the contrary (Fig. 7a), shows considerable sub-structure of much higher surface brightness. The brightest feature is an elliptical component of  $30 \times 14$  mas, and 140 mJy, from which two elongated and curved features ("jets"?) are emerging.

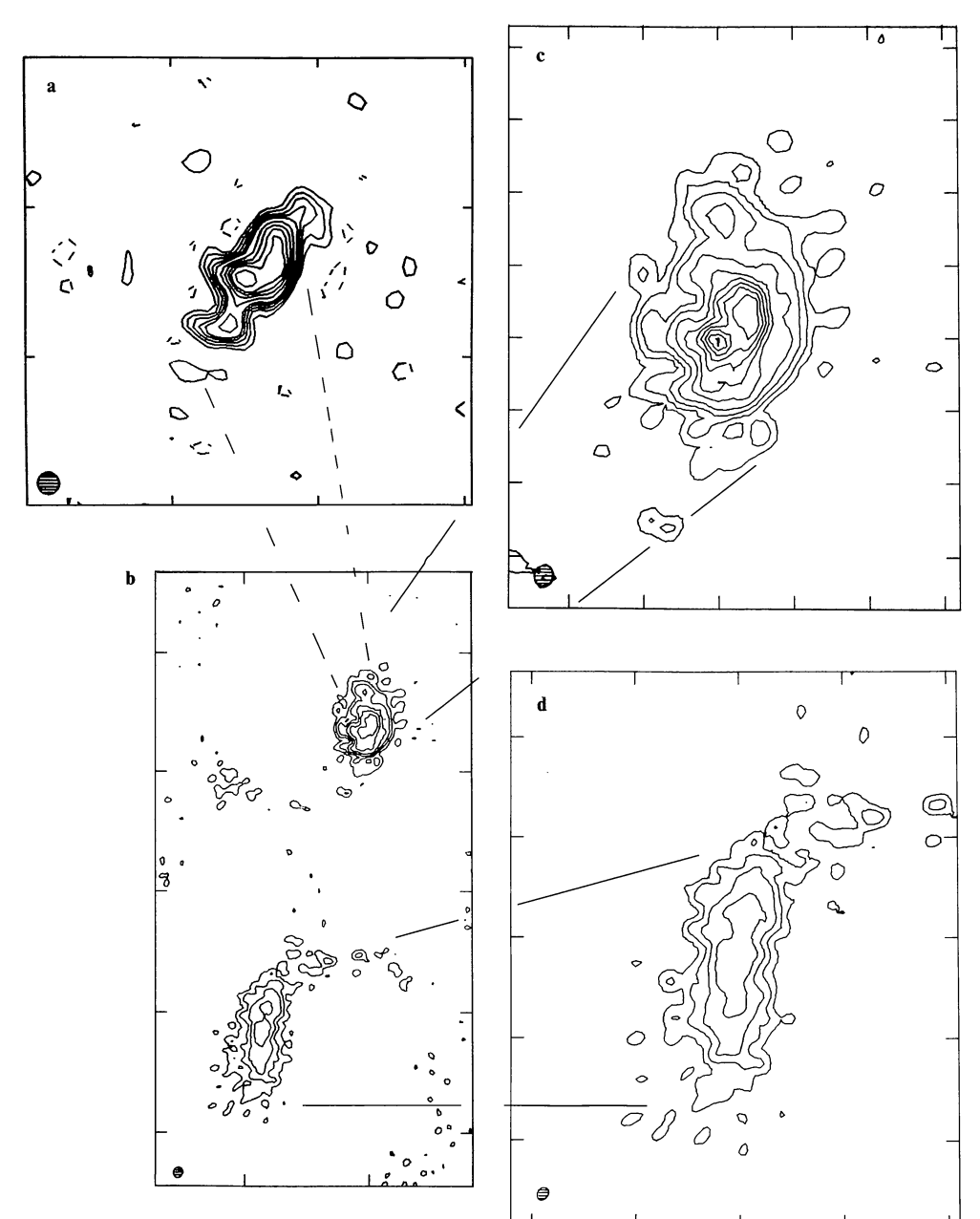


Fig. 7a–d. Brightness distribution at 1.6 GHz of 3C 268.3. a EVN data (northern component); beam:  $30 \times 30$  mas; tick separation: 200 mas; contours:  $4.2 \times (-1, 1, 2, 3, 4, 5, 7.5, 10, 12.5, 15, 20)$  mJy/beam; peak flux: 110 mJy/beam; b–d: EVN + MERLIN data; b Whole source; c northern component; d southern component; beam:  $26 \times 24$  (p.a. = -25) mas; tick separation: 500 mas in b, 100 mas in c and 200 mas in d; contours:  $2.5 \times (-2, 1, 2, 4, 8, 16, 32)$  mJy/beam in b;  $2.0 \times (1, 2, 4, 8, 16, 32, 40, 48, 56, 64)$  mJy/beam in c;  $2 \times (1, 2, 4, 8)$  in d; peak flux: b and c 131 mJy/beam, d 30 mJy/beam

In Fig. 7b we present the map obtained combining the EVN and MERLIN data. The bright features of the northern component are well visible in this map (Fig. 7c); furthermore a broad, uniform and low brightness "halo" shows up. The southern component (Fig. 7d) instead does not present any compact feature.

At 6 cm vBMH find 7% linear polarization in the southern component but do not detect any polarization at either 6 or 2 cm in the northern one. Both components have an overall straight steep spectrum ( $\alpha > 1.0$ ) from 18 to 2 cm. The asymmetry in surface brightness and polarization leads to the suggestion (as for 3C 49 and 3C 67) that the northern component may contain the true "core". The optical position of the suggested identification (Laing et al., 1983) is closer in declination to the northern component than to the southern one (or to the mid point), but it seems far from

either component in right ascension. A better optical position is needed.

 $3C\ 287$ : Single complex structure (Fig. 8). The resolution of the present map is not enough to see the structure in detail. However there is a clear change in the source position angle in going towards its centre. This change is even more evedent from inspection of the visibilities along the u-v tracks: it is clear that the maxima and minima of the visibility amplitudes at different baselines do not line up, implying that the long and short baselines "see" differently oriented structures.

The brightness peak itself is off center indicating some possible projection effects. Within the calibration uncertainties, the present map accounts for the total flux density at 18 cm, hence no low brightness extended feature is likely to have been resolved out. The

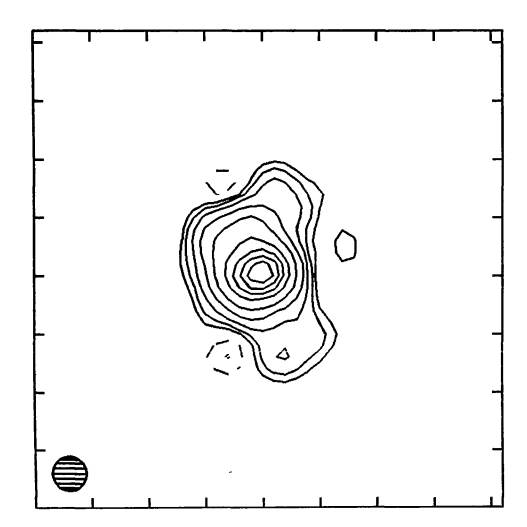


Fig. 8. Brightness distribution at  $1.6 \,\text{GHz}$  of  $3C\,287$ . Beam:  $30 \times 30 \,\text{mas}$ ; tick separation:  $50 \,\text{mas}$ ; contours:  $26.4 \times (-2, -1, 1, 1, 2, 4, 8, 16, 32, 48, 64, 80) \,\text{mJy/beam}$ ; peak flux:  $2640 \,\text{mJy/beam}$ 

shape of 3C 287 suggests that it may be a curved "core-jet" seen end-on. This might indicate that the relativistic beaming should play a role in this source. However the absence of a dominant core is a problem with this interpretation. Perley (1982) and vBMH find about 5% polarization at 6 and 2 cm respectively.

3C 303.1: The source is largely resolved by the EVN baselines, accounting at most (EF-DW) for 50% of the total flux density.

The EVN map, presented in Fig. 9a, shows a broad elliptical structure some  $100 \times 40$  mas in size, containing three more compact knots, from which an elongated feature emanates westward (and possibly a second fainter and shorter one eastward).

Figure 9b shows the combined EVN+MERLIN map. The western feature now appears as a "jet" extending to a larger distance and some further emission of lower brightness is also evident. The orientation of the "jet" is at p.a. -70 deg.

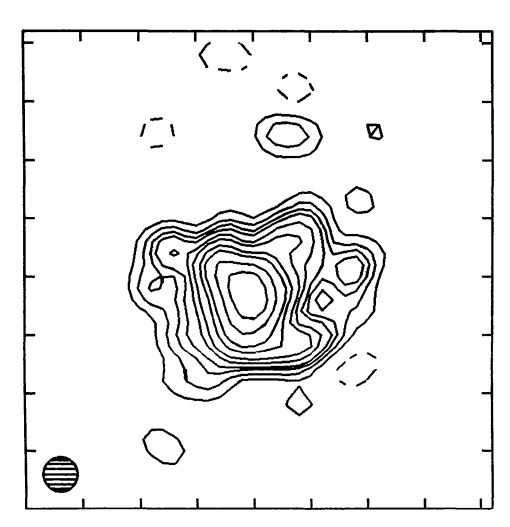


Fig. 10. Brightness distribution of 3C 343 at 1.6 GHz. Beam:  $30 \times 30$  mas; tick separation: 50 mas; contours:  $7.4 \times (-2.5, 2.5, 5, 7.5, 10, 15, 20, 30, 40, 60, 80)$  mJy/beam; peak flux: 740 mJy/beam

The very faint component at  $\sim 1.\%$  in p.a.  $-41 \, \text{deg}$  is the remnant of an elongated low brightness feature, well visible at MERLIN resolution, and is misaligned with respect to the "western jet" by about 20 deg.

Some 100 mJy are still missing from the combined EVN + MERLIN map, which may be ascribable to the component 1.78 away. The plots of the visibility amplitudes and closure phases are given in Fig. 12c).

 $3C\,343$ : The morphology is very complex (Figs. 10 and 12d). The brightness distribution is centrally peaked but several ridges of emission can be seen along different position angles. A component, with 5–10% of the map peak flux, is present  $\sim 150$  mas north of the emission peak, well detached from the main emitting region; however we are not sure about the reality of such a component. The map accounts for all the source flux density.

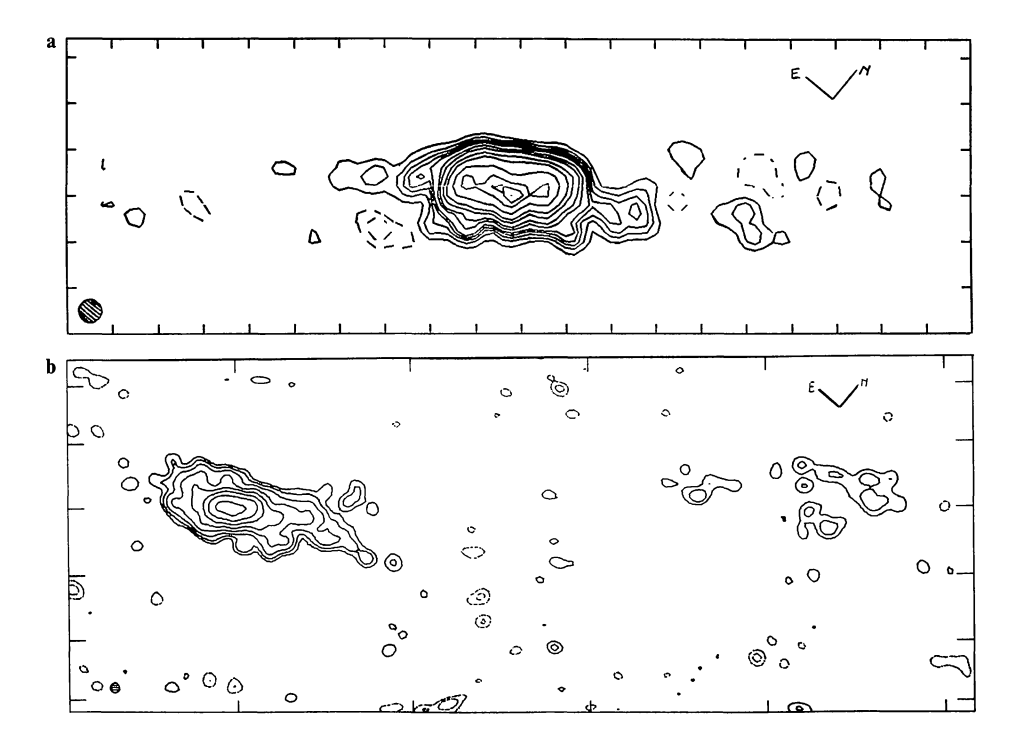


Fig. 9a and b. Brightness distribution at  $1.6\,\mathrm{GHz}$  of  $3\,\mathrm{C}\,303.1$ . a EVN data; beam:  $25\times25\,\mathrm{mas}$ ; tick separation:  $50\,\mathrm{mas}$ ; contours:  $1.8\times(-2,-1,1,2,3,4,5,7.5,10,15,20,30,40)\,\mathrm{mJy/beam}$ ; peak flux:  $90\,\mathrm{mJy/beam}$ . b EVN+MERLIN data: beam:  $25\times25\,\mathrm{mas}$ ; tick:  $500\,\mathrm{mas}$  in R.A. and  $200\,\mathrm{in}$  dec; contours:  $1.0\times(-2,-1,1,2,4,8,16,32,64,128)\,\mathrm{mJy/beam}$ ; peak flux:  $170\,\mathrm{mJy/beam}$ . Note: the two maps are rotated by  $40\,\mathrm{deg}$  clockwise

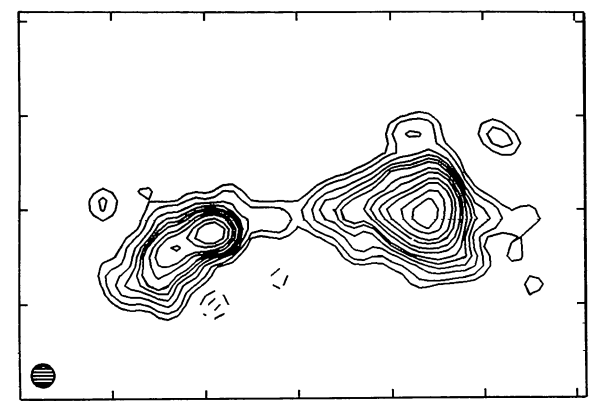


Fig. 11. Brightness distribution of 3C 343.1 at 1.6 GHz; Beam:  $25 \times 25$  mas; tick separation: 100 mas; contours:  $4.4 \times (-2, -1, 1, 2, 4, 6, 8, 10, 15, 20, 30, 40, 60, 80)$  mJy/beam; peak flux: 440 mJy/beam

The source is undetected in the survey by Pearson and Readhead (1981), which excludes the presence of a compact core at a level of ~300 mJy at 5 GHz. Like 3C 287 this could also be a "core-jet" source seen end-on, although the same comment about beaming effects apply here. Perley (1982) and vBMH find 1.1 and 4% linear polarization at 6 and 2 cm respectively.

 $3C\,343.I$ : Complex double source (Fig. 11). The two components have very different shapes and both contain high brightness features. The map accounts for  $\sim 90\%$  of the total flux density.

At 2 cm, VLA measurements by vBMH do not resolve either component, neither is any polarization detected. Both components have a straight steep spectrum ( $\alpha \sim 0.9$ ) between 18 and 2 cm.

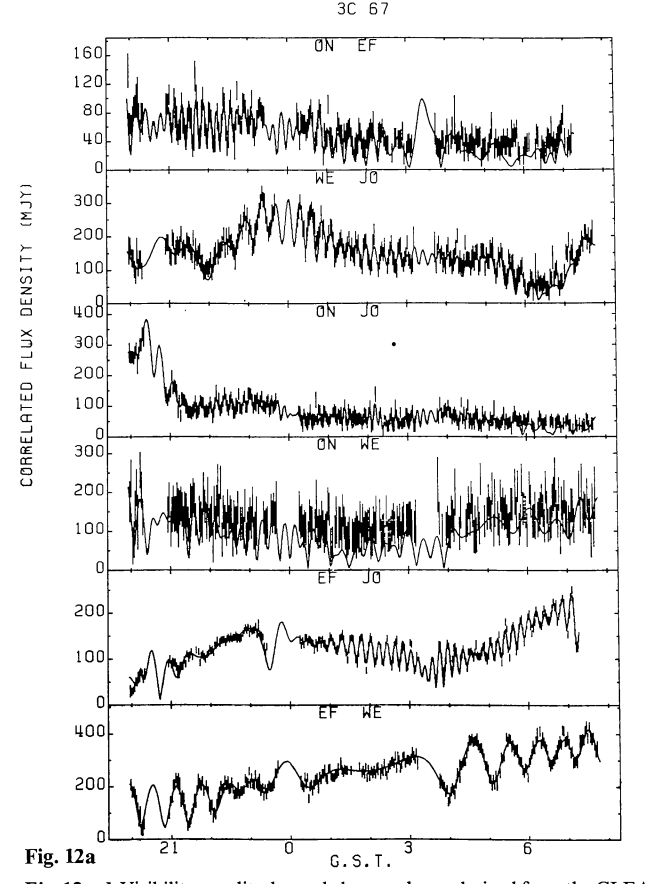
#### 6. Discussion

Although the observations of this sample are still incomplete and mostly at one frequency only, we wish to discuss briefly a few items which we consider important for this class of radio source.

## 6.1. Morphological composition of the sample

A rough classification of 15 of the 18 C-sources in the sample can be made on the basis of our data, supplemented by published work. We find:

	3C 119
267 2237 2241 2268.3 2298	3C 287 3C 303.1 3C 343
	2237 2241 2268.3 2298



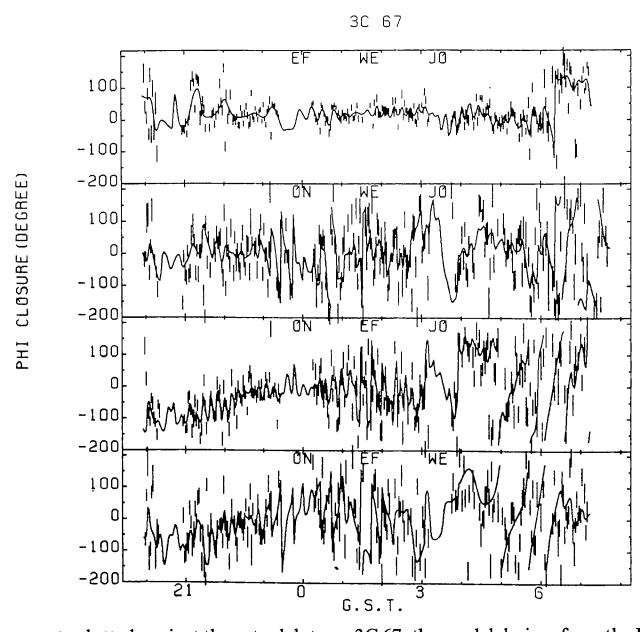
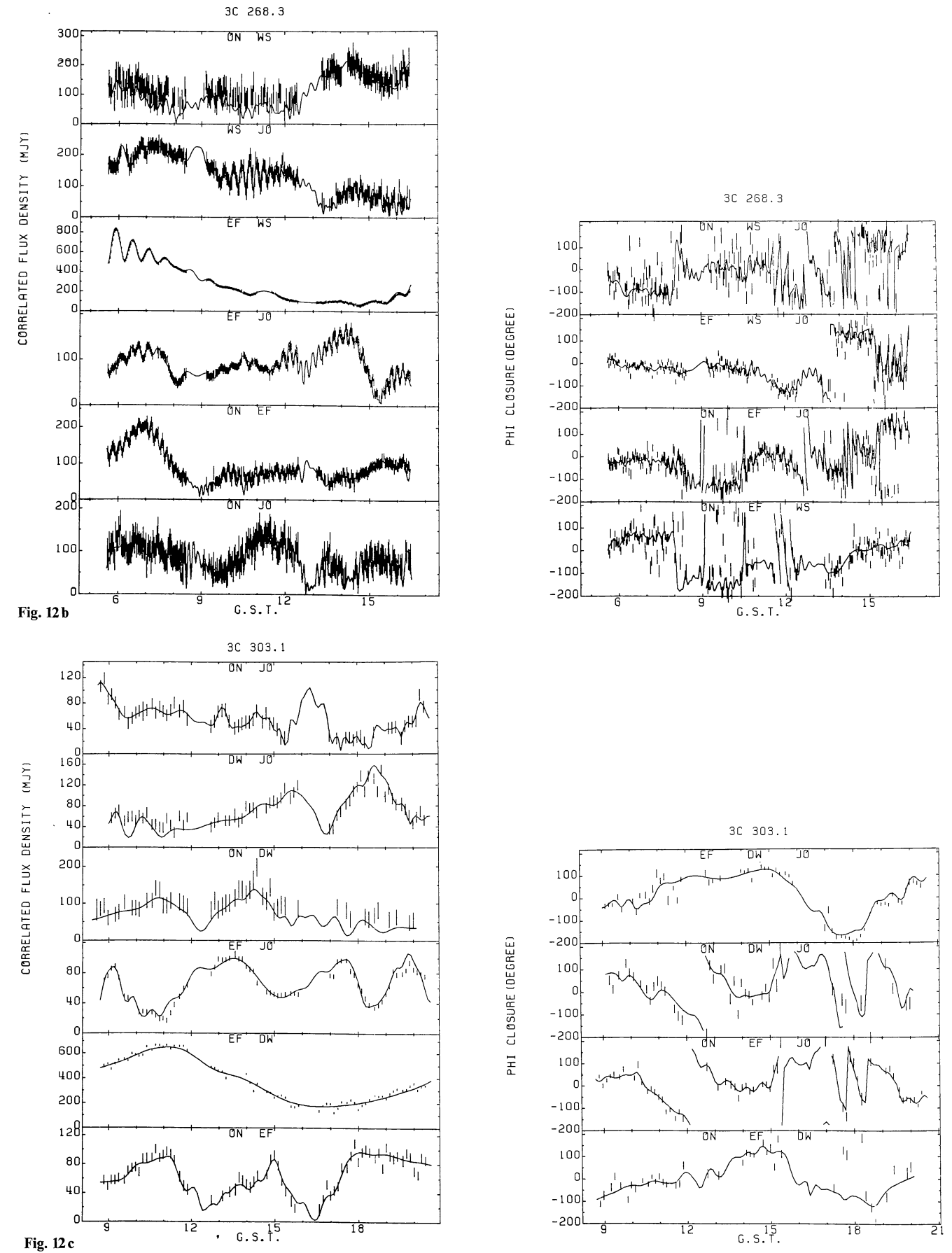
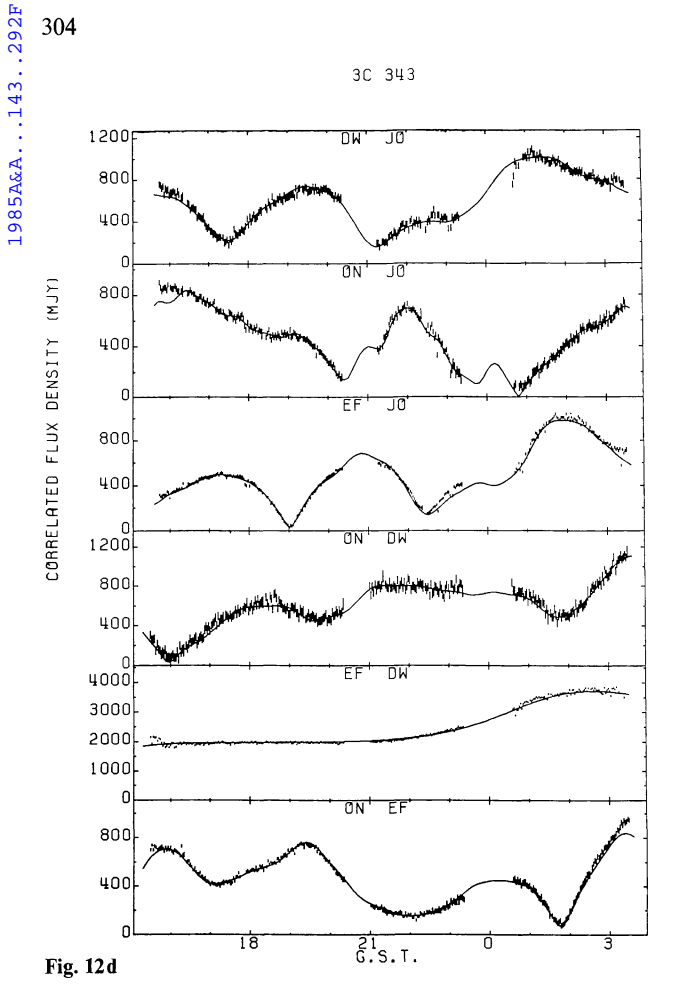


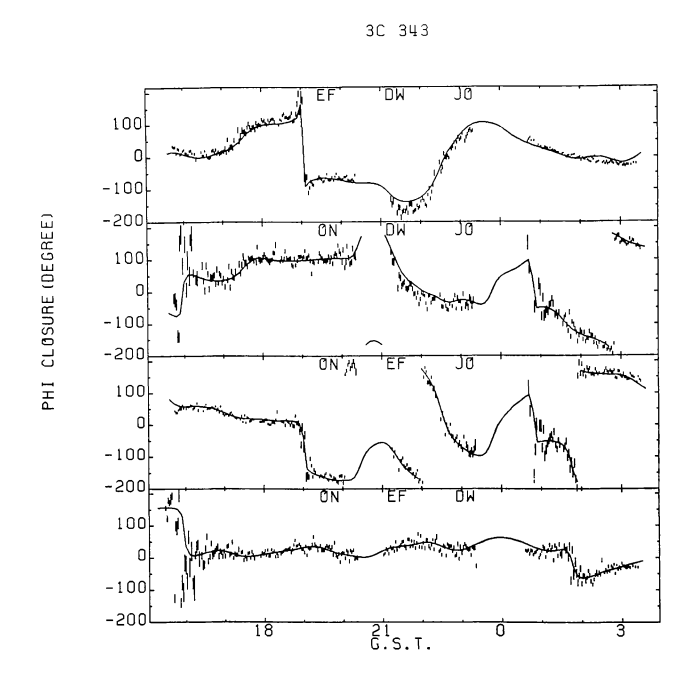
Fig. 12a-d. Visibility amplitudes and closure phases derived from the CLEAN components plotted against the actual data. a: 3C 67: the model derives from the EVN + MERLIN data; b: 3C 268.3: the model derives from the EVN + MERLIN data; c 3C 303.1; d 3C 343











It is emphasized that the above morphological classification is crude and could well be proven to be wrong in the light of new data with better sensitivity and/or resolution. See for instance (reference in Table 1) how the morphological description of 3C 147 changes with the type of observations.

Some of the doubles (e.g. 3C 237, 3C 241) could be similar to the compact doubles found by Phillips and Mutel (1982), although a factor ten more extended. Actually, when observed with a number of beam/source comparable to the one used by those authors, these sources appear remarkably symmetric. Moreover their spectrum bends at a lower frequency, as expected if, when moving away from their origin, the radio lobes evolve and expand to larger sizes, becoming more and more optically thin (Phillips and Mutel, 1982).

A large uncertainty in the morphological classification derives from the current lack of multi-frequency data, which might allow reliable identification of a flat spectrum core (if it exists) with one of the source subcomponents. Some of the doubles could actually be asymmetric (i.e. D2 type) sources with one component being the core (e.g. 3C49) or containing the core (e.g. 3C67 and perhaps 3C 268.3). In this case they could be related to the core-jet class. In complex cases like 3C 287 and 3C 343 the determination of a core location would greatly help in the interpretation of the radio structure.

A quick examination of the above classification shows that quasars are either "core-jet" type or complex, while all galaxies except 3C 303.1 are doubles, although not necessarily simple doubles. Analogous results, based on a similar sample of sources mapped with MERLIN, have been already pointed out by Wilkinson et al. (1984b).

## 6.2. Collimation

Even accounting for the uncertainties in the source classification, it seems that in several cases we are dealing with structures showing unstable direction of ejection or little, if any, collimation. Noteworthy are: 3C 147, discussed by Wilkinson (1984), where at least three different directions of ejection from the radio core seem to occur (Preuss et al., 1982); 3C287 and 3C343, in whose overall amorphous structures, large changes of position angle (or multiple position angles) are observed; 3C 303.1, where the two streams emerging from the rather broad elliptical component indicate that collimation is taking place on kpc scales, definitely at a considerable distance from the "central engine", wherever it is. Cases like 3C 287 and 3C 343 could perhaps be thought of as "core-jet" structures seen end-on, in which projection effects can greatly enhance small intrinsic distortions. However the absence of a strong flat spectrum core would not be in agreement with relativistic beaming models.

Considering that these radio sources have sub-galactic sizes, vBMH suggest an interesting scenario (see also Allan, 1984: Wilkinson et al., 1984a), where the radio morphology is determined by propagation of jets through a dense and inhomogeneous interstellar medium. The jets collide with gas clouds and perhaps entrain, heat and accelerate the ambient gas. This might account for the bright radio emission and distorted morphology and several other radio and optical properties of CSS sources.

## 6.3. Low frequency turnover

The low frequency turnover in these sources is often assumed to be due to synchrotron self-absorption. It has been pointed out that this interpretation, coupled with the measured small source sizes, would lead to abnormally low estimates of the magnetic fields (Cotton, 1983) and consequently to high electron densities. This would be the situation where Inverse Compton scattering is the relevant process. We consider such an interpretation premature at least in the case of the present sources, since we have single frequency maps only. A proper interpretation requires multifrequency mapping, in order to: a) measure component sizes at a frequency as close as possible to the turnover frequency; b) determine the spectral indices of the individual components. The present observations at 1.66 GHz could be blind to broad steep spectrum components dominating at low frequencies and actually responsible for the turnover.

Recently, an alternative interpretation of the spectral turnover has been suggested by vBMH in terms of free-free absorption of the radio emission by the same gas clouds which are responsible for the (forbidden) narrow line emission. This hypothesis is based on the finding that the narrow line regions (NLR) and the radio sources seem to have about the same linear size and that, in some cases, also morphological similarities have been found (Miley, 1981). Such an interpretation seems plausible and should lead in the future to interesting comparative studies between multi-frequency radio maps and high resolution optical images obtained with the Space Telescope.

# 6.4. Unified scheme

In the unified scheme of Orr and Browne (1982), the steep spectrum of the CSS sources could be understood if the structures are not aligned close to the line of sight, and therefore the cores are not subject to Doppler boosting due to relativistic beaming. The non-dominant-core-jet category of CSS sources could be evidence for jet emission which is not moving relativistically, the so-called "disembodied" jets (Moore, 1984; see also Browne, 1984).

Alternatively, they could be objects seen end-on which have an abnormally high ratio of the jet (steep spectrum) to the core (flat spectrum) flux, so as to be steep spectrum objects. One can imagine several mechanisms able to produce such an effect, but it is not appropriate to discuss them here. In several cases, however, the morphologies we see do not resemble jets at all, either seen parallel or perpendicular to the line of sight. Furthermore, double sources reminiscent of the "compact doubles" of Phillips and Mutel, are also present in our sample. It is possible that the selection criteria adopted work in the direction of selecting objects of different nature which, for different reasons, are compact with a steep spectrum.

Further observational work is required to disentangle the problem and to establish whether the CSS objects are a link between the compact flat spectrum and the extended steep spectrum sources.

Acknowledgements. We are grateful to Dr. M. Charlsworth and Dr. R. E. Spencer for permission of using the MERLIN data before publication.

We thank the staff of the observatories involved in this experiment for their assistance with the observations. We also

thank H. Blaschke, U. Stursberg, and Luedeke of the MPI für Radioastronomie for their help in running the MK-II processor in Bonn, and J. D. Romney, R. W. Porcas, D. A. Graham, and W. Alef for their assistance in the use of pre-mapping software.

The drawings and photographs have been carefully prepared by L. Baldeschi and R. Primavera.

The Netherlands Foundation for Radioastronomy is supported by the Netherlands Organization for the Advancement of Pure Research (ZWO).

#### References

Allan, P.M.: 1984, Astrophys. J. 276, L31

Barthel, P.D., Schilizzi, R.T., Miley, G.K., Jägers, W.J., Strom, R.G.: 1984, Astron. Astrophys. (submitted)

Browne, I.W.A.: 1984, *Proc.* IAU *Symp.* 110, Reidel, Dordrecht, p. 1

Bridle, A.H., Fomalont, E.B.: 1978, Astron. J. 83, 704

Bridle, A.H., Fomalont, E.B., Cornwell, T.J.: 1981, *Astron. J.* **86**, 1294

Bracewell, R.: 1954, Australian J. of Physics 7, 615

Broderick, J.J., Condon, J.J.: 1975, Astrophys. J. 202, 596

Clark, R.W., Broten, N.W., Legg, T.H., Locke, J.L., Yen, J.L.: 1969, Monthly Notices Roy. Astron. Soc. 146, 381

Clark, T.A., Erickson, W.C., Hutton, L.K., Resch, G.H., Vandenberg, N.R., Broderick, J.J., Knowles, S.H., Youmans, A.B.: 1975, Astron. J. 80, 923

Cohen, M.H., Moffet, A.T., Romney, J.D., Schilizzi, R.T., Shaffer,
D.B., Kellermann, K.I., Purcell, G.H., Grove, G., Swenson,
G.W., Yen, J.L., Pauliny-Toth, I.I.K., Preuss, E., Witzel, A.,
Graham, D.: 1975, Astrophys. J. 201, 249

Cornwell, T.J., Wilkinson, P.N.: 1981, Monthly Notices Roy. Astron. Soc. 196, 1067

Cotton, W.: 1983, Astrophys. J. 271, 51

Davies, J.G., Anderson, B., Morison, I.: 1980, Nature 288, 64

de Bruyn, A.G., Wilson, A.S.: 1978, Astron. Astrophys. 64, 433

Geldzahler, B., Fanti, C., Fanti, R., Schilizzi, R.T., Shaffer, D., Weiler, K.W.: 1984a, Astron. Astrophys. 131, 232

Graham, D., Matveienko, L.I.: 1984, *Proc. IAU Symp.* 110, Reidel, Dordrecht, p. 43

Heckman, T.M., Miley, G.K., van Breugel, W.J.M., Butcher, H.: 1981, Astrophys. J. 247, 403

Heckman, T.M., Miley, G.K., Balick, B., van Breugel, W.J.M., Butcher, H.: 1982, Astrophys. J. 262, 529

Jenkins, C.J., Pooley, G.G., Riley, J.M.: 1977, *Mem. Roy. Astron.* Soc. **84**, 61

Joshi, M.N., Gopal-Krishna: 1977, Monthly Notices Roy. Astron. Soc. 178, 717

Kapahi, V.K.: 1981, Astron. Astrophys. Suppl. 43, 381

Kellermann, K.I., Pauliny-Toth, I.I.K., Williams, P.J.S.: 1969, Astrophys. J. 157, 1

Kuhr, H., Nauber, U., Pauliny-Toth, I.I.K., Witzel, A.: 1979,
Preprint No. 55 of Max-Planck-Institut für Radioastronomie
Kus, A.J., Wilkinson, P.N., Booth, R.S.: 1981, Monthly Notices
Roy. Astron. Soc. 194, 527

Laing, R.A.: 1981, Monthly Notices Roy. Astron. Soc. 194, 301Laing, R.A., Riley, J.M., Longair, M.S.: 1983, Monthly Notices Roy. Astron. Soc. 204, 151

MacDonald, G.H., Miley, G.K.: 1971, Astrophys. J. 164, 237 Miley, G.K.: 1980, Ann. Rev. Astron. Astrophys. 18, 165

Miley, G.K.: 1981, Proc. on "Optical Jets in Galaxies", ESA SP-162, p. 9

- Moore, P.K.: 1984, Monthly Notices Roy. Astron. Soc. (submitted)
  Orr, M.J.L., Browne, I.W.: 1982, Monthly Notices Roy. Astron.
  Soc. 200, 1067
- Peacock, J.A., Wall, J.V.: 1982, Monthly Notices Roy. Astron. Soc. 198, 843
- Perley, R.A.: 1982, Astron. J. 87, 859
- Pearson, T.J., Readhead, A.C.S., Wilkinson, P.N.: 1980, Astrophys. J. 236, 714
- Pearson, T.J., Readhead, A.C.S.: 1981, Astrophys. J. 248, 61 Pearson, T.J., Readhead, A.C.S.: 1984, Proc. IAU Symp. 110, Reidel, Dordrecht, p. 15
- Phillips, T.J., Mutel, R.L.: 1982, Astron. Astrophys. 106, 21
- Phillips, R.B., Shaffer, D.B.: 1983, Astrophys. J. 271, 32
- Preuss, E., Alef, W., Pauliny-Toth, I.I.K., Kellermann, K.I.: 1982, Proc. IAU Symp. 97, Reidel, Dordrecht, p. 289
- Preuss, E., Alef, W., Whyborn, N., Wilkinson, P.N., Kellermann, K.I.: 1984, IAU Symp. 110, Reidel, Dordrecht, p. 29
- Readhead, A.C.S., Wilkinson, P.: 1980, *Astrophys. J.* 235, 11 Scheuer, P.A.G., Readhead, A.C.S.: 1979, *Nature* 277, 182
- Simon, R.S., Readhead, A.C.S., Moffet, A.T., Wilkinson, P.N., Anderson, B.: 1980, Astrophys. J. 236, 707
- Simon, R.S., Readhead, A.C.S., Moffet, A.T., Wilkinson, P.N., Allen, B., Burke, B.F.: 1983, *Nature* 302, 487

- Simon, R.S., Readhead, A.C.S., Wilkinson, P.N.: 1984, *IAU Symp*. 110, Reidel, Dordrecht, p. 111
- van Breugel, W.J.M.: 1984, IAU Symp. 110, Reidel, Dordrecht, p. 59
- van Breugel, W.J.M., Heckman, T.A., Miley, G.K.: 1984a, *Astrophys. J.* 276, 79
- van Breugel, W.J.M., Heckman, T.A., Butcher, H., Miley, G.K.: 1984b, Astrophys. J. 277, 82
- van Breugel, W.J.M., Miley, G.K., Heckman, T.: 1984c, Astron. J. 89, 5 (vBMH)
- Wilkinson, P.N., Readhead, A.C.S., Purcell, G.K., Anderson, B.: 1977, Nature 269, 764
- Wilkinson, P.N., Readhead, A.C.S.: 1979, Astrophys. J. 232, 365Wilkinson, P.N.: 1982, Proc. IAU Symp. 97, Reidel, Dordrecht, p. 149
- Wilkinson, P.N.: 1983, Proc. Intern. Conf. VLBI Techniques, Toulouse
- Wilkinson, P.N., Booth, R.S., Cornwell, T.J., Clark, R.R.: 1984a, *Nature* **308**, 619
- Wilkinson, P.N., Spencer, R.E., Readhead, A.C.S., Pearson, T.J., Simon, R.S.: 1984b, Proc. IAU Symp. 110, Reidel, Dordrecht, p. 25
- Wilson, A.S., Willis, A.G.: 1980, Astrophys. J. 240, 429